PNAS
www.pnas.org

Supplementary Information for

Modulation of a protein-folding landscape revealed by AFM-based force spectroscopy notwithstanding instrumental limitations

Devin T. Edwards[a], Marc-Andre LeBlanc[a], Thomas T. Perkins[a,b,1]

Corresponding Author: Thomas T., Perkins
E-mail:tperkins@jila.colorado.edu

This PDF file includes:

Supplementary Information Text

Materials and methods

Protein expression. We developed a polyprotein (Fig. 2*A*) and probed this polyprotein with a cantilever functionalized with the protein cohesin. Both proteins required expression. The plasmid to express ybbR-tagged cohesin was graciously provided by Prof. Hermann Gaub and his lab. The plasmid used to express the polyprotein was based on the pET28a vector. The starting vector was also provided by the Gaub lab. It included an N-terminal ybbR tag (1) for surface anchoring followed by a 6X-His tag for Ni^{2+} affinity purification. It also included ddFLN4 from *Dictyostelium discoideum,* previously characterized by AFM (2). At the C-terminus was type-III dockerin along with its stabilizing X-module from *Ruminococcus flavefaciens*, which allowed for strong attachment to type-III cohesin on the AFM cantilever (3). α_3D was inserted into this plasmid between the ddFLN4 and the dockerin using Gibson assembly (4). Briefly, both DNA encoding α_3D, obtained by gene synthesis (Genscript), and the vector were PCR amplified with individually designed primers (Integrated DNA Technologies) that contained complementary overlapping regions. The fragments were combined using the Gibson Assembly Cloning Kit (New England BioLabs, NEB) and amplified in *E. Coli* strain XL 10-Gold cells (Agilent Technologies). In a subsequent step, ddFLN4 was replaced by a pair of NuG2 marker domains. The sequence for a pair of NuG2 proteins was taken from a previously prepared plasmid (5). Both this sequence and the vector were amplified with primers that again contained complementary overlapping regions. The fragments were combined using NEBuilder HIFI DNA assembly kit (NEB) and amplified in NEB 5-alpha Competent E. coli (NEB). A longer polyprotein was generated by inserting ~40 nm of an elastin-like-polypeptide (ELP) that was previously used as linkers in AFM force spectroscopy (6). We acquired a 50-amino-acid segment (~20 nm contour length) of this ELP via a vector deposited into Addgene's plasmid database (Addgene #90472). The protein sequence amplified out of the plasmid was:

VPGEGVPGVGVPGVGVPGVGVPGVGVPGAGVPGAGVPGGGVPGGGVPGEG

The same NEBuilder HIFI assembly process inserted this sequence both before the NuG2 marker domains and after α_3D. Due to the repetitive nature of the sequence, we did this insertion in two steps and verified the sequence in between.

The ybbR-tagged cohesin, the polyprotein, and the extended polyprotein were prepared identically. *E. Coli* strain BL21 (DE3) cells were transformed with the plasmid, streaked on agar plates, and then single colonies selected for growth and overexpression via an autoinduction buffer (7). To do so, we autoclaved 1 L of autoinduction media (pH 7.2) containing 6 g Na_2HPO_4, 3 g KH_2PO_4, 20 g Tryptone, 5 g yeast extract, and 5 g NaCl. We then filter sterilized a sugar stock containing 10 mL 60% v/v glycerol, 5 mL of 10% w/v glucose, and 25 mL of 8% w/v lactose. A single colony was picked and grown in autoinduction media supplemented with sugar stock (40 mL per L) and kanamycin (100 μg/ml). Cultures were grown overnight at 37 °C with 200 RPM shaking. Cells were harvested and resuspended in Lysis buffer [25 mM Tris (pH 8.0), 150 mM

NaCl, 1 mM PMSF] before lysis by sonication. Lysate was clarified and nutated for 30 min with a 2 mL packed Ni-NTA column (HisPure, Thermo) equilibrated with 25 mM Tris (pH 8.0), 150 mM NaCl. The column was washed with 5 column volumes (CV) of wash buffer [25 mM Tris (pH 8.0), 150 mM NaCl, 20 mM imidazole, 1 mM PMSF) before elution with 3 CV of elution buffer [25 mM Tris (pH 8.0), 150 mM NaCl, 200 mM imidazole, 1 mM PMSF]. The eluted protein was dialyzed into the AFM assay buffer [25 mM HEPES (pH 7.0), 150 mM NaCl]. Protein was aliquoted and snap-frozen and stored at −80 °C until needed.

Cantilever calibration. Prior to functionalization, cantilevers were calibrated in air using the thermal method (8). Briefly, the detector sensitivity was determined through hard contact with a glass or mica surface. The power-spectral density (PSD) of the zero-force cantilever deflection was then collected by averaging at least 300 measurements down to 50 Hz at a fixed stage height. PSDs were collected with the cantilever at an extremum of the sinusoidal optical-interference artifact at a typical distance >2 μm above the surface (9). The PSD was fit to a simple-harmonic oscillator model to determine k. For these cantilevers, the k measured at positive and negative extrema of the artifact were the same within our error, but a systematic variation can be observed for larger interference artifacts. The stiffness was calculated 3–5 times for each cantilever at different surface locations. The average stiffness was then used for the cantilever throughout the experiments.

Coverslip and cantilever functionalization. We prepared functionalized glass coverslips and AFM cantilevers using silane-PEG-maleimide [MW_{PEG} = 600 (PG2-MLSL-600, Nanocs)] following established protocols (10), and then incubated with Coenzyme A (CoA) to create stable, CoA-functionalized cantilevers and coverslips. In advance of functionalization, 12-mm glass coverslips (Ted Pella, 26023) were sonicated in acetone and ethanol for 5 min each. Coverslips were etched for 3 min in a 3M KOH solution of 75% Ethanol/25% deionized water (DI water, >18.2 MΩ). Coverslips were then rinsed in 2 L of DI water and sonicated in a second beaker of DI water for 3 min. Slides were blown dry with dry N_2 and stored in an airtight box. Immediately prior to functionalization, AFM cantilevers were rinsed for 15 s each in DI water, isopropanol, toluene, isopropanol, and DI water before being blotted dry.

Cleaned cantilevers and coverslips were placed in a UV-ozone chamber (Novascan) for 30 min. They were then incubated in 0.15 mg/ml silane-PEG-maleimide in toluene for 3 h at 60 ºC. A stir bar and custom-fabricated holders facilitated gentle agitation to improve surface homogeneity. After 3 h, cantilevers and coverslips were rinsed for 15 s in each of toluene, isopropanol, and DI water. To avoid degradation of maleimide reactivity, the cantilevers and coverslips were immediately incubated with 1 mM CoA (C3019, Sigma-Aldrich) dissolved in 50 mM sodium phosphate (pH 7.5), 50 mM NaCl, 10 mM EDTA. Incubation proceeded at room temperature for >1 h after which the cantilevers and coverslips were stored at 4 ºC in humidity chambers for 2–4 weeks.

Site-specific protein conjugation. On the day of experiment, the ybbR-tagged cohesin protein was conjugated to the CoA-functionalized cantilevers, and the polyprotein (Fig. 2*A*) was conjugated to the CoA-functionalized glass coverslips. In both cases, this conjugation was enzymatically catalyzed by Sfp phosphopantetheinyl transferase (Sfp) (1). To do so, we first rinsed off any remaining CoA solution from the cantilevers or coverslips by repeated submersing into ~100 mL of DI water. The cantilevers and coverslips were then carefully blotted dry. Using 5-min epoxy, coverslips were bonded to 15-mm metal pucks (Ted Pella, 16218) used to mount the sample in our commercial AFM. Polyprotein conjugation was performed in AFM assay buffer supplemented with ~5 μM Sfp and 25 mM $MgCl_2$ by adding in small volumes (~1 μL) of concentrated stocks. We note that these concentrations were not optimized and likely far higher than was necessary for activity. We incubated the cantilevers with 20 μM ybbR-tagged cohesin to saturate the cantilever tip. In contrast, we incubated the coverslips with ~25–250 nM of the polyprotein since we preferred a low surface concentration to avoid multiple attachments. Surface conjugation proceeded at room temperature for ~1 h. The cantilevers were then rinsed 3 times with 10 mL of the AFM assay buffer before placing the cantilever into ~25 mL of buffer for 2 min. Cantilevers were then stored in ~40 μL of AFM assay buffer with 1 mM $CaCl_2$ added to increase the longevity of the attachment chemistry (11). Coverslips were rinsed in ~10 mL of AFM assay buffer and then 5 mL of AFM assay buffer + 1 mM $CaCl_2$.

AFM assay. After loading the cantilever and sample, we let the instrument settle for 30 min and then used the stiffness value of the precalibrated cantilever in determining the detector sensitivity (V/nm) based on a fit to the thermal noise spectrum. To attach the tip to the polyprotein, we performed a grid-based search of the surface during which the tip was brought into gentle contact (~100 pN) with the surface for 0.1 s and rapidly retracted at a moderate velocity (*e.g.*, v = 400 nm/s). A real-time trigger was used to screen for potential attachment by stretching the polyprotein to fully unfold α_3D and the pair of NuG2 but not enough to rupture the cohesin-dockerin interface (*e.g.*, F > 40 pN at x_{meas} > 120 nm). This real-time trigger indicated a molecular attachment and the cantilever was returned to within a few nm of the surface.

If the resulting force-extension curve indicated pulling on a single-molecule, an automated centering routine was performed by moving the surface sequentially along the x- and y-axes while holding the unfolded polyprotein under constant force (80–120 pN) (12). Under such a constant force feedback loop, lateral displacement of the surface led to the vertical motion of the cantilever base as the polyprotein was stretched at an angle. A fit to the resulting parabolic shape yielded the maxima in cantilever displacement and thereby located the position where the attachment point of the polyprotein to the coverslip was directly under the attachment point to the cantilever. This centering routine was run twice. We note that this routine significantly improved the precision and accuracy of the assay because we were studying the first domain to unfold and the linkers were quite short. This regime was quite different from the canonical protein-unfolding AFM assay that stretches a polyprotein consisting of 8 identical domains (13).

Once the tip was attached to a single polyprotein and aligned vertically, we collected a full series of both dynamic and equilibrium data on a single, individual molecule over ~10–60 min. The duration of an attachment to an individual molecule was primarily limited by detachment of the polyprotein from the tip or acquiring multiple attachments that generally could only be remedied by detaching entirely from the construct. To assure that a single-molecule was interrogated over this extended period, the polyprotein was fully unfolded and refolded at constant velocity regularly during the experiment (Fig. S1). To account for vertical drift, we occasionally touched off the surface. The automated centering routine was repeated every ~5–10 min to account for lateral drift between the tip and the sample. Finally, the sum signal on the quadrant photodiode was kept approximately constant at ~7 volts and the laser position reoptimized periodically, as needed.

Dynamic data was collected by moving the base of the cantilever back and forth at a constant velocity using four different velocities (v = 20, 50, 100, and 400 nm/s). A single dynamic trace was composed of numerous cycles at a constant velocity where the extension range was chosen to ensure α_3D unfolded and refolded in each cycle while minimizing the probability of unfolding the NuG2 marker domains. The number of cycles per trace varied based on velocity and the distance traveled. We kept the total trace time less than ~100 s to minimize the impact of residual force drift (14).

Equilibrium data were recorded by pausing the base of the cantilever at a constant position (Z_{cant}) where the folded and unfolded states were nearly equally populated. A semi-automated process was used identify Z_{cant} to account for variations in attachments. To do so, we measured the variance of the deflection signal as Z_{cant} was stepped through the unfolding transition of α_3D. The variance increased in regions where α_3D was both folded and unfolded. We estimated Z_{equil} from the peak of this variance. α_3D's dynamics were then measured at $Z_{cant} = Z_{equil}$ - 0.4 nm, $Z_{cant} = Z_{equil}$, and $Z_{cant} = Z_{equil}$ + 0.4 nm to account for uncertainty in Z_{equil}. Data were collected for 5 s at each extension, with a 0.2-s dwell near the surface between each extension to embed a set of zero force references to account for residual force drift. We repeated this several times for each attachment to ensure high-quality records with nearly equal populations of the folded and unfolded state. All equilibrium data reported in Fig. 3 were taken using the same cantilever to improve precision (15).

Allan deviation. We calculated force precision of the cantilever by selecting a portion of the equilibrium data in a single state. We then calculated the Allan deviation using $\sigma_x(T) = \sqrt{\frac{1}{2}\left\langle (\overline{x}_{i+1} - \overline{x}_i)^2 \right\rangle_T}$ where $\overline{x}_i$ is the mean value of the data over the i^{th} time interval T (16).

Equilibrium lifetime analysis. We analyzed equilibrium traces using a Hidden-Markov model (HMM) as discussed in the Materials and Methods. Some smoothing was necessary to achieve good discrimination between states. However, the HMM model produced consistent folding rates across a range of smoothing levels with only a weak dependence on the degree of smoothing applied. Decimation of the data was found to be necessary to achieve good fitting. Specifically,

we smoothed the 50-kHz data with a 21-point 2nd order Savitzky-Golay filter and decimated by a factor of 10.

To determine rates on a molecule-by-molecule basis, we used data from traces that had populations between 44 and 56% in the folded state. To account for limited ability to detect short-lived states, we imposed a hard cut-off and discarded lifetimes below 1 ms and then calculated the average folding and unfolding rates from the inverse of the mean lifetimes for each trace. An analytic correction to the rates was then applied to account for the applied 1 ms cutoff (17). We averaged the unfolding and folding rate to determine an average transition rate for each trace, as these rates were approximately equal. The average rate from all traces at a given pH was subsequently calculated. The reported error was the standard error of the mean (SEM). Due to variations in the number of traces that conformed to our 44–56% acceptable range and the extended interrogation time (~10–60 min), sometimes more than one 5-s trace was analyzed from the same molecule.

To calculate the cumulative distribution functions, we used all the lifetimes >1 ms from traces that conformed to our acceptable population range. These were rank sorted from shortest (n = 1) to longest ($n = n_{tot}$) where n_{tot} is the total number of lifetimes. We then plotted these lifetimes along the x-axis with the y-axis given by $\frac{n_{tot}-n}{n_{tot}}$. An exponential fit was used to measure the decay times for the cumulative distributions. These decay times agreed with the average rates determine above.

Rate map analysis. To generate rate maps from dynamic data, we aligned the force-extension curves and then identified where transitions occurred. To start with, the data from an individual cycle of stretching and relaxing the polyprotein was analyzed only if during that individual cycle neither of the NuG2 domains unfolded. Next, to account for slow force drift over a full set of cycles contained in a single trace (~100 s), we used the set of short dwells near the surface to demark F = 0. Force-extension curves within a trace were found to overlap well after this correction and generally no further correction was applied.

We aligned sets of force-extension curves from different traces using worm-like chain (WLC) fits to the portions of the force-extension curves corresponding to α_3D being folded and unfolded. Specifically, an early force-extension curve was used as a reference. A WLC fit was performed by concurrently fitting the folded and unfolded states of α_3D from this curve. The WLC parameters for the two states were held identical, except for the contour length. The contour length difference between the folded and unfolded state was successful in describing the data when allowed to vary from 22–25 nm [encompassing the 23 nm canonical value (10)]. Note, at the low unfolding forces of α_3D (<15 pN), this change in contour length (ΔL_0) was not as sharply constrained by the WLC fitting as typically occurs when studying more mechanically robust proteins that rupture at higher F. Small force and extension offsets were allowed but were identical for both states. Finally, small manual shifts were applied to fully overlap the curves, as needed.

Following alignment, we next identified the location of folding and unfolding transitions in the dynamic data by identifying the folding or unfolding transition time. First, smoothed force data was passed thru a simple step-finding algorithm (https://github.com/thomasbkahn/step-detect). The level of smoothing and the step threshold were empirically tuned to yield good results. Optimal parameters varied from molecule to molecule and velocity to velocity.

These automatically detected transition times were manually corrected and supplemented to account for missed or mislocated states. To ensure the transitions times were not biased by use of smoothed data, we algorithmically determined the transition time. This determination was done by identifying two small regions immediately before and after the estimated transition. We then fit a line to the data in the region before and after the transition and determined the reported transition time from when the 50 kHz data last crossed the first fit line before arriving at the second line for the first time.

To calculate the force-dependent folding and unfolding rates [$k_{ij}(F)$], we used the following formula from (17)

$$k_{ij}(F) = \frac{N_{ij}(F)}{t_i(F)} \quad (1)$$

where $N_{ij}(F)$ is the number of transitions from state i to state j at F, and $t_i(F)$ is the total occupation time of state i at force F. This formula is a slight modification of that proposed by Zhang and Dudko (18).

To improve the precision in determining the force at which a transition occurred, we generated a single WLC fit for the folded and unfolded state of all traces at a single velocity. The transition time determined above was then used to determine the molecular extension at the transition time based on a linear fit of the extension around the transition. This effective average extension was then used to determine the rupture force from the WLC fit for the appropriate state. These folding and unfolding forces were then binned into a histogram using a width of 1 pN for unfolding forces and 0.5 pN for folding to generate $N_{ij}(F)$.

As with the equilibrium life-time analysis, we used an analytic correction to account for limited temporal resolution (17). Our hard cutoff was again 1 ms, based on our ability to detect state lifetimes of 1 ms (Fig. S5). Note, this 1-ms temporal value was the effective temporal resolution needed to discriminate between states and distinct from the mechanical response time of the cantilevers (~30 μs). We therefore eliminated state lifetimes that were shorter than 1 ms. To apply this analytic correction, we proceeded in two steps. First, we accounted for missing transitions out of briefly occupied states by adjusting rates via

$$k_{mol} = \frac{k_{obs}}{1 - k_{obs}\tau_{cutoff}} \quad (2)$$

where k_{mol} is the corrected rate, k_{obs} is the measured rate, and τ_{cutoff} = 1 ms is the dwell time cutoff. This formula corrects fast rates for missed transitions due to the limited temporal capabilities of our experiments.

For every transition out of an unresolved short-lived state, we must include a transition into that state out of the corresponding long-lived state. We calculated the number of missed transitions via

$$N_{\mathrm{miss}} = (e^{k_{\mathrm{mol}}\tau_{\mathrm{cutoff}}} - 1)k_{\mathrm{obs}}\tau_{\mathrm{i}}. \quad (3)$$

These missed transitions occur on the opposite branch of the rate map. We therefore mapped N_{miss} into the corresponding force bin. To do so, we assumed that the missed transitions should be placed homogeneously into the mapped force bins (17). Once we added the new transitions into the proper bins, we recalculated $k_{ij}(F)$ to determine the corrected rates. We discarded bins containing fewer than 5–10 rupture events at a single velocity. Rates occurring above 250 s^{-1} were not used in the analysis due to the 1-ms cutoff. Resulting rate maps for each molecule at pH 6.2 and pH 4.2 are shown in Fig. S7.

Calculation of ΔG_0: We calculated ΔG_0 from individual equilibrium traces following Yu *et al.* (19) using

$$\Delta G_0 = -k_{\mathrm{B}}T \ln\left(\frac{P_{\mathrm{U}}}{P_{\mathrm{F}}}\right) - \Delta G_{\mathrm{cant}} - \Delta G_{\mathrm{linker}} - \Delta G_{\mathrm{released}} \quad (4)$$

where k_BT is the thermal energy, and P_F and P_U are the populations in the folded and unfolded states determined from the HMM fits. In the traces analyzed, P_F varied from 0.44 to 0.56 in line with our analysis for rates. ΔG_{cant} is the work performed by the cantilever upon unfolding

$$\Delta G_{\mathrm{cant}} = \frac{1}{2\,k}(F^2_{\mathrm{folded}} - F^2_{\mathrm{unfolded}}) \quad (5)$$

where F_{folded} and $F_{unfolded}$ are the average forces measured in the folded and unfolded state. These values were determined from the peak locations of force histograms of data smoothed to ~200 Hz. ΔG_{linker} is the work done relaxing the linkers in the polyprotein from F_{folded} to $F_{unfolded}$

$$\Delta G_{\mathrm{linker}} = \int_{x_{\mathrm{linker}}(F_{\mathrm{folded}})}^{x_{\mathrm{linker}}(F_{\mathrm{unfolded}})} F_{\mathrm{WLC}}(x, L_0)dx. \quad (6)$$

This linker energy corresponds to stretching the originally unstructured polymer chain in the assay (x_{linker}). $F_{WLC}(x, L_0)$ is the WLC force as a function of extension (x) with contour length L_0 of the folded state. L_0 is determined from WLC fits to the folded state of force-extension curves. $x_{linker}(F)$ is the extension of the folded state at a certain force, which is determined from the same WLC model. $\Delta G_{unfolded}$ is the work to stretch the polypeptide that is released when α_3D unfolded

$$\Delta G_{\mathrm{unfolded}} = \int_0^{x_{\mathrm{released}}(F_{\mathrm{unfolded}})} F_{\mathrm{WLC}}(x, \Delta L_{\mathrm{c}})dx \quad (7)$$

where ΔL_0 is the released contour length, which was determined from WLC fits to the folded and unfolded states of force-extension curves, as described above. Good agreement was found with ΔL_0 restricted to be 22–25 nm, consistent with the 23-nm canonical unfolding distance (10).

For each equilibrium trace, we calculated ΔG_0. This included 12 traces over six molecules at pH 6.2 and 14 traces over 3 molecules at pH 4.2. Average values were ΔG_0 = 14.8 ± 0.2 k_BT (average ± SEM) at pH 6.2 and ΔG_0 = 11.9 ± 0.4 k_BT at pH 4.2. Although a small change in stability was detected at low pH, we used the average value across all traces for generating landscapes ΔG_0 = 13.5 ± 0.3 k_BT.

Calculation of D_{meas} and k_A: Calculation of D_{meas} followed previous work of Cosio *et al.* (20) and Neupane *et al.* (21). In brief, we used

$$D_{\mathrm{meas}} = \frac{\langle \delta x_{\mathrm{meas}}^2 \rangle}{\tau}, \tag{8}$$

where $\langle \delta x_{\mathrm{meas}}^2 \rangle$ is the variance of the extension data in a state, and τ is the characteristic decay time of the autocorrelation of the extension data in that state. For this calculation, we used data collected at 500 kHz for the modified cantilever and 50 kHz for the uncoated BioLever Long to ensure unbiased sampling of the distribution of extensions. We note that incorrect measurement of stiffness based on inadvertent smoothing of force probe motion was a common problem in early efforts to calibrate the stiffness of optical traps (22). We examined three 5-s traces on three molecules at pH 6.2. The HMM analysis was used to divide the trace into dwells in individual states. D_{meas} was then calculated for each of these states. We then restricted this analysis to states lasting longer than 10 ms to avoid any problems of analyzing extremely brief states. We found the difference in averages of D_{meas} for the folded and unfolded states was <2%. Averaging D_{meas} for these three molecules yielded D_{meas} = 2.3×10^4 nm^2/s ± 200 nm^2/s for the modified cantilever. We note that when calculating D_{meas} using 50-kHz data, this value slightly decreased to 1.8×10^4 nm^2/s ± 250 nm^2/s, indicative that the response of the modified cantilever was slightly smoothed even at 50 kHz digitization. We repeated this calculation for a gold-etched BioLever Long using a single equilibrium trace, which yielded 3.1×10^3 nm^2/s. We illustrate this calculation in Fig. S11.

We next calculated the rate of diffusion over the landscape assuming Kramers equation (23) using

$$k_{\mathrm{A}} = \frac{1}{2\pi k_{\mathrm{B}}T}\sqrt{\kappa_{\mathrm{barrier}}\kappa_{\mathrm{well}}}D_{\mathrm{meas}}\exp(-\beta\Delta G_{\mathrm{A}}^{\ddagger}/k_{\mathrm{B}}T) \tag{9}$$

where ΔG_A is the barrier height in the landscape, and $\kappa_{barrier}$ and κ_{well} are the curvatures of the barrier and the well, respectively. We determined the landscape parameters from the landscapes reconstructed with the inverse-Weierstrass transform (IWT). We determined the curvature by fitting the barrier and the folded well to $\frac{1}{2}k\,(x-x_0)^2 + y_0$, where k is the stiffness of the feature, and x_0 and y_0 are offsets.

The resulting averages were k_A = 171 ± 06 s^{-1} (average ± SEM) at pH 6.2 and k_A = 199 ± 5 s^{-1} at pH 4.2. Due to the small difference in these values, we report k_A = 179 ± 5 s^{-1}, averaged over all the IWT landscapes. We note that this calculation was done based on constant-force landscapes tilted to $F_{1/2}$. However, our equilibrium assay was not done under constant force, but rather at constant cantilever height. This leads to a significant acceleration in the observed rates (24).

Calculating entropic landscapes. Entropic landscapes were computed based on the energy needed to stretch a system composed of two states of different contour lengths where the elasticity of each state was modeled as a WLC. Following Hummer and Szabo (25), we modeled the free-energy profile from the linkers alone $[G_0(x)]$ in our experiment from

$$e^{-G_0(x)/k_BT} = e^{-G_1(x)/k_BT} + e^{-G_2(x)/k_BT} \quad (10)$$

where $G_1(x)$ and $G_2(x)$ are the free-energy landscape for the folded and unfolded state. ΔG_0 (= 13.5 k_BT) set the vertical offset between $G_1(x)$ and $G_2(x)$ at x = 0. As shown in Fig. 5*A*, the resulting landscape does not show a barrier. However, when the landscape was tilted to $F_{1/2}$ where both minima had the same energy, a small barrier (~1.5 k_BT) was observed (Fig. 5*A*, inset). This calculation was repeated for different molecules with different initial tether lengths, which resulted in different barrier heights (Fig. S9).

	Stiffness (pN/nm)
Transition state stiffness (IWT)	1.9 ± 0.1
Folded state stiffness (IWT)	0.76 ± 0.03
Force probe	5.2–6.4
AFM linker stiffness at rupture (F = 10 pN)	0.75
Optical-trapping linker stiffness (F = 10 pN)	0.5

Table S1. Stiffness values for the assay. The typical stiffness for a variety of parameters in pN/nm. The folded and transition state stiffnesses were determined by fits to the IWT landscapes. Force probe stiffnesses are taken directly from experimentally determined cantilever stiffnesses. AFM and optical trap linker stiffnesses at rupture were modelled using a WLC model evaluated at 10 pN in the folded state of α3D for the AFM and at 10 pN in 600-nm DNA with a persistence length of 42 nm (26) and a stretch modulus of 1200 pN (27) for the optical trap. The stiffness associated with a typical optical-trapping assay added as a point of comparison.

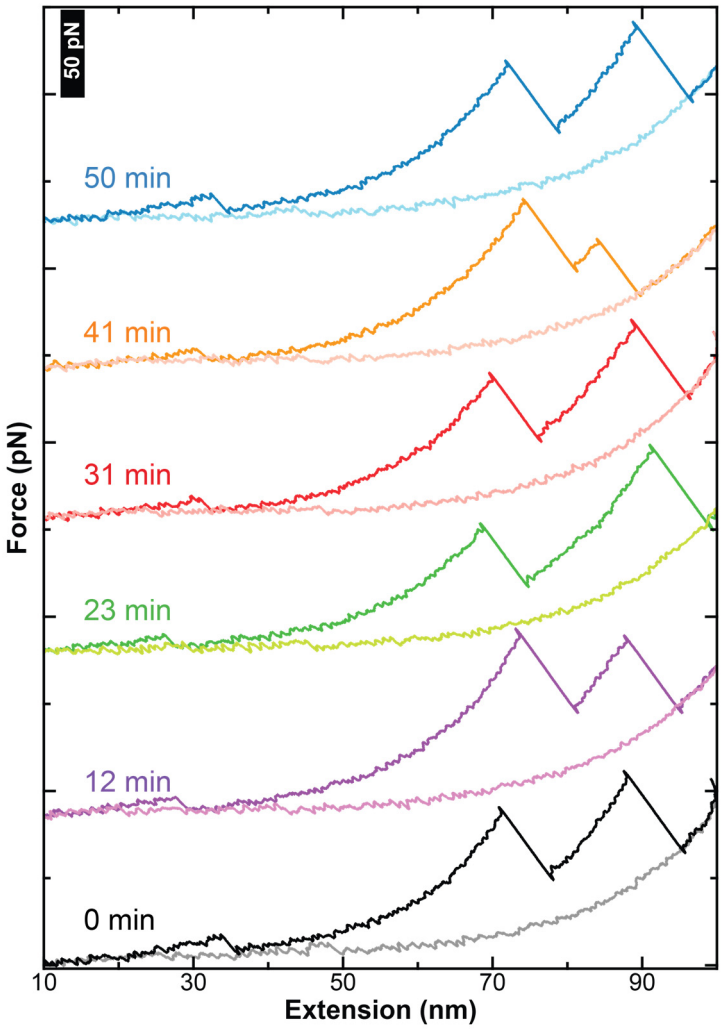

Fig. S1. Studying an individual molecule for tens of minutes. Six representative force-extension curves acquired from a single molecule studied over the course of >50 min. Each stretching curve (dark color) is accompanied by its subsequent relaxation curve (light color). Traces offset vertically for clarity. Data smoothed to 200 Hz. Note that these traces, which depict full unfolding of the entire polyprotein, were acquired periodically to check for multiple attachments. For quantifying the dynamics of α_3D, the range of the cantilever motion was restricted to just unfold α_3D, as shown in Fig. 4A.

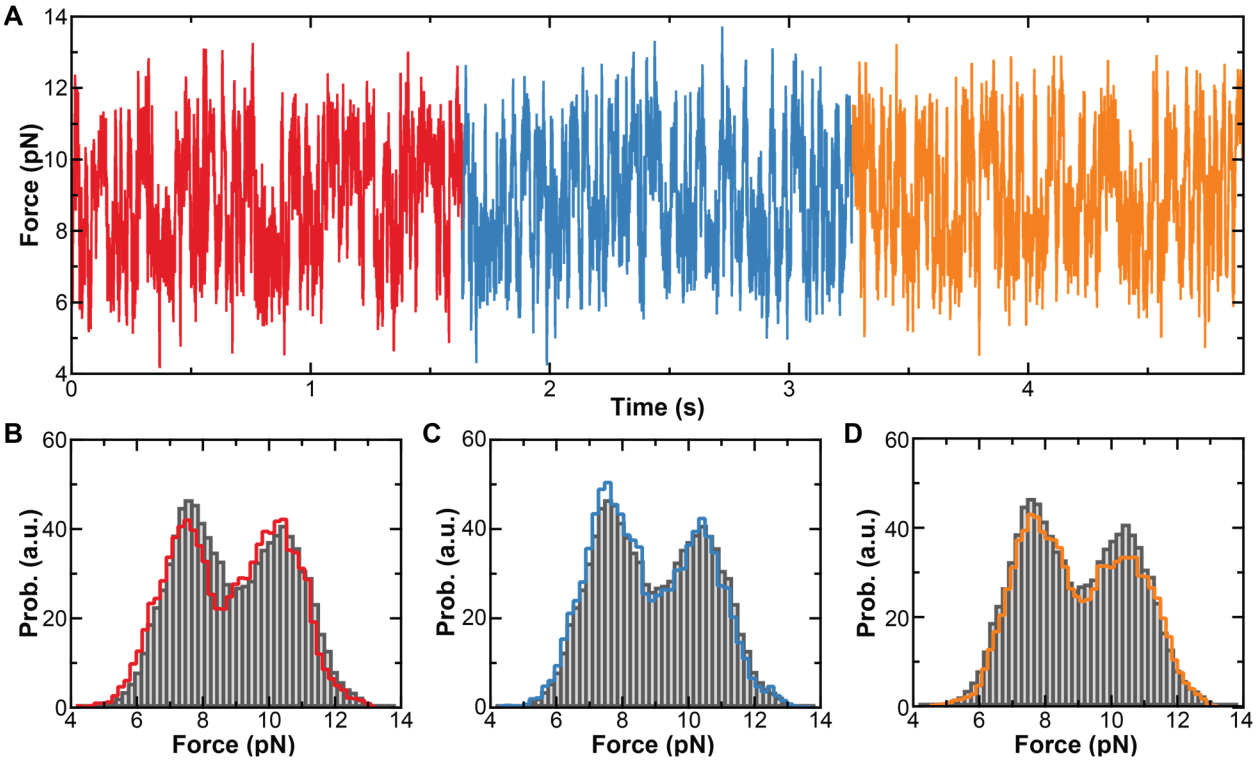

Fig. S2. Force stability demonstrated by showing stable occupation of folded and unfolded states over time. (**A**) Force-vs-time plot of α_3D at a fixed base position of the cantilever at pH 4.5. Data smoothed to 200 Hz. Colored regions divide the record into thirds. (**B**–**D**) Probability densities of forces calculated for the first (*red*), second (*blue*), and final (*orange*) thirds of the trace shown in panel A. Grey bars represent the force probability density of the entire trace.

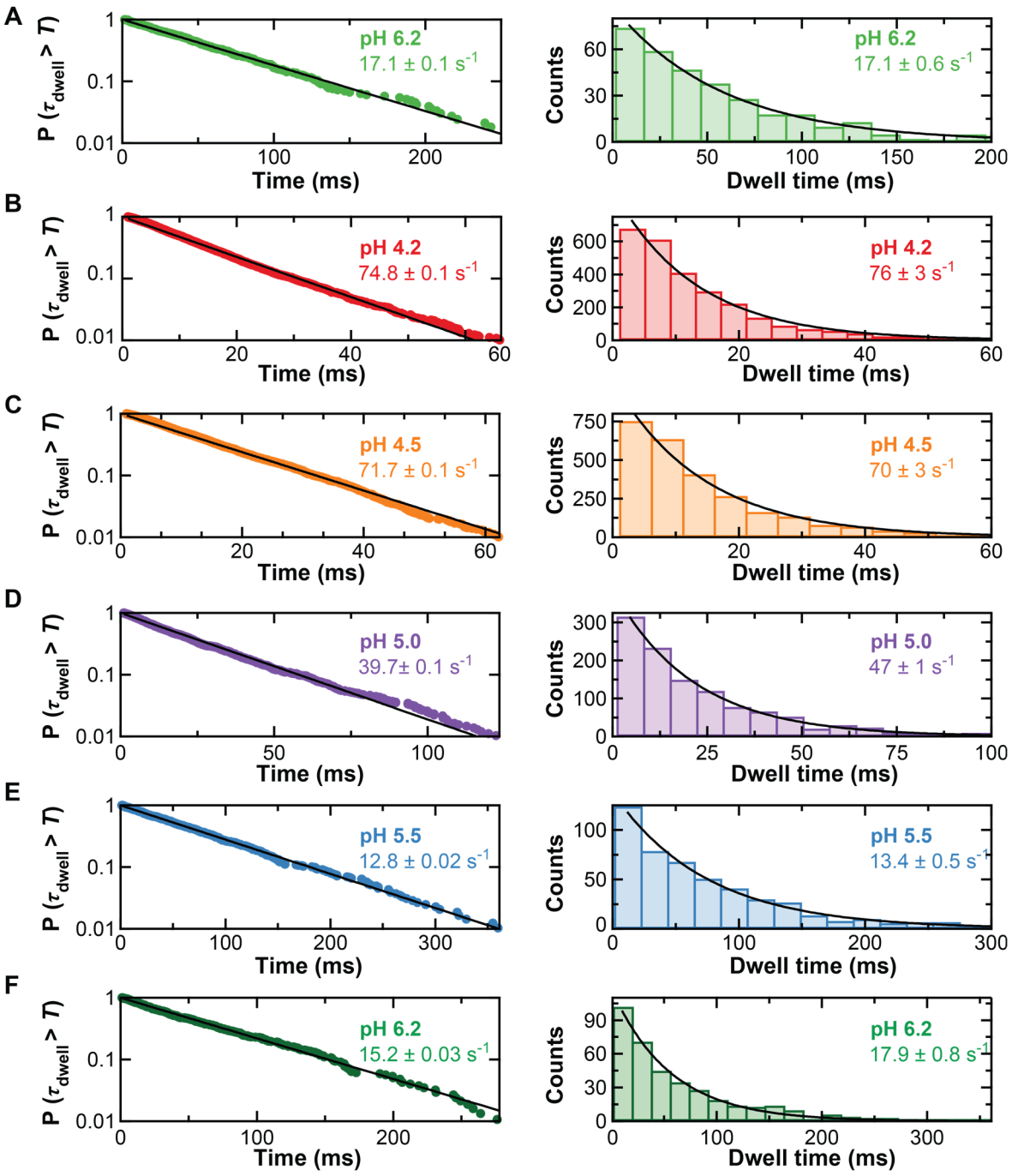

Fig. S3. Equilibrium records show exponentially distributed state lifetimes. Normalized cumulative distribution functions (left) and state lifetime histograms (right) at different pH values. These graphs were computed by combining the folded and unfolded state lifetimes across multiple molecules at (**A**) pH 6.2 [green, (N_{mol} = 3, $N_{transitions}$ = 335)]; (**B**) pH 4.2 [red, (N_{mol} = 3, $N_{transitions}$ = 2782)]; (**C**) pH 4.5 [orange, (N_{mol} = 2, $N_{transitions}$ = 2678)]; (**D**) pH 5.0 [purple, (N_{mol} = 3, $N_{transitions}$ = 1170)]; (**E**) pH 5.5 [blue, (N_{mol} = 3, $N_{transitions}$ = 494); (**F**) pH 6.2 [dark green, (N_{mol} = 2, $N_{transitions}$ = 379)]. The reported lifetimes for each panel were determined by an exponential fit and the error given by the uncertainly in the fitting parameter.

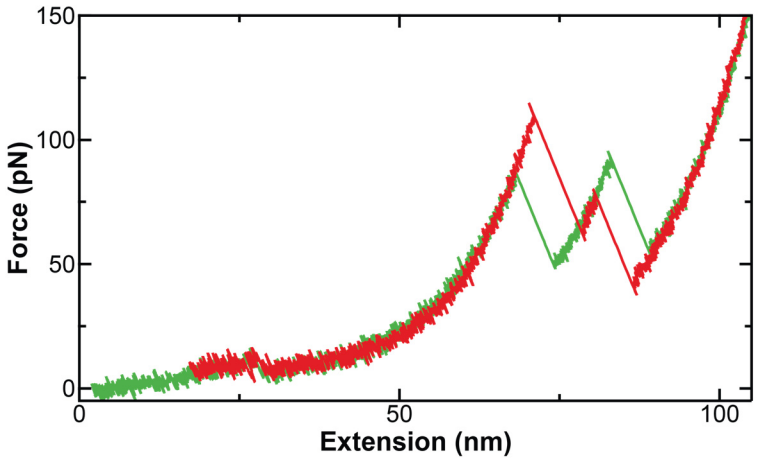

Fig. S4. Elasticity of the polyprotein consistent at neutral and low pH. Force-extension curves showing the unfolding of the polyprotein construct at pH 6.2 (green) and pH 4.2 (red).

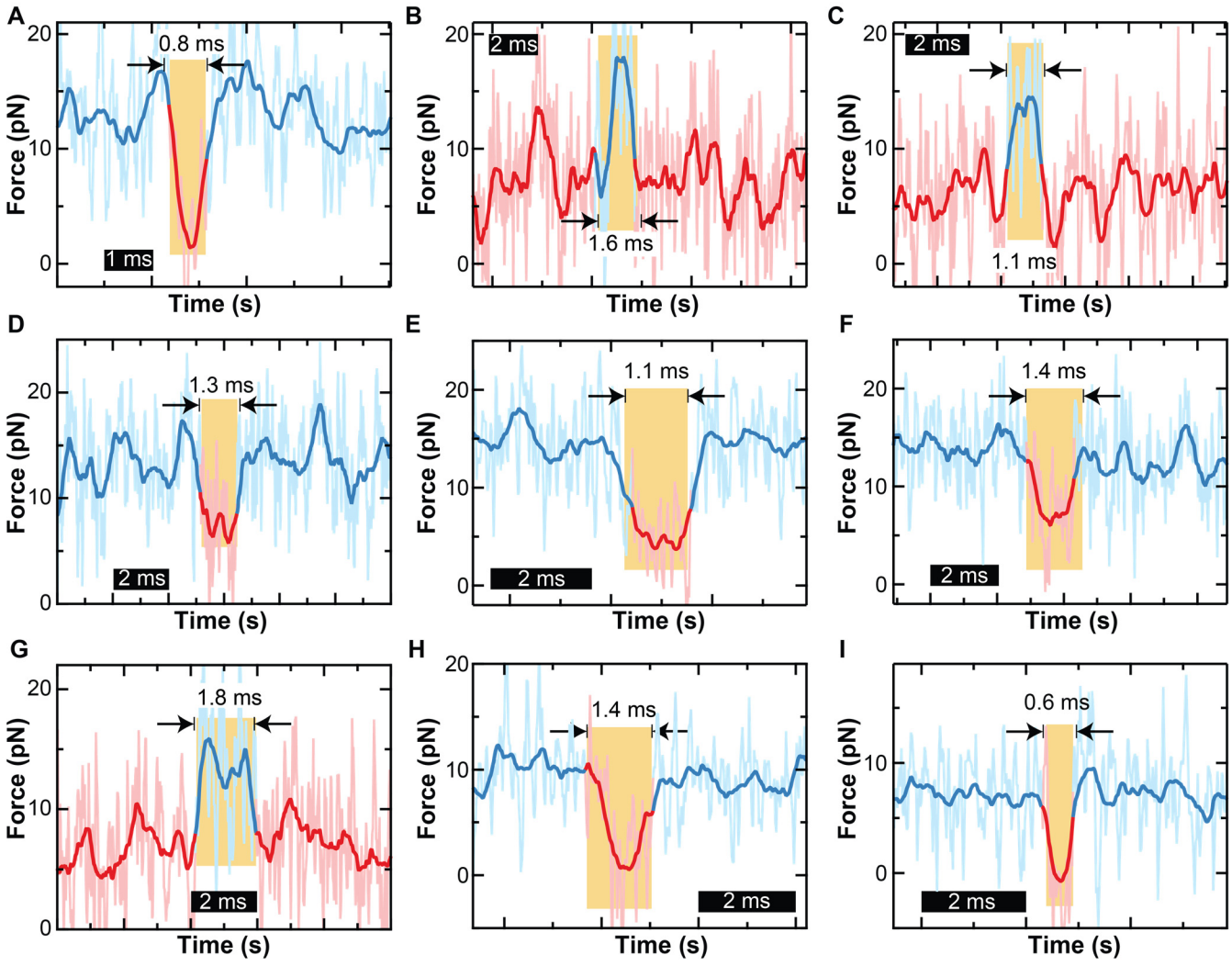

Fig. S5: Modified cantilevers resolved state lifetimes of 1 ms. (**A**–**I**) Individual high-resolution force-vs-time records showing brief dwell times in unfolded (red), and folded (blue) states. Data displayed at 50 kHz (light colors) and 1 kHz (dark colors). Data acquired while the cantilever base was moving so brief unfolding events well below the mean unfolding force were occasionally observed (panel I).

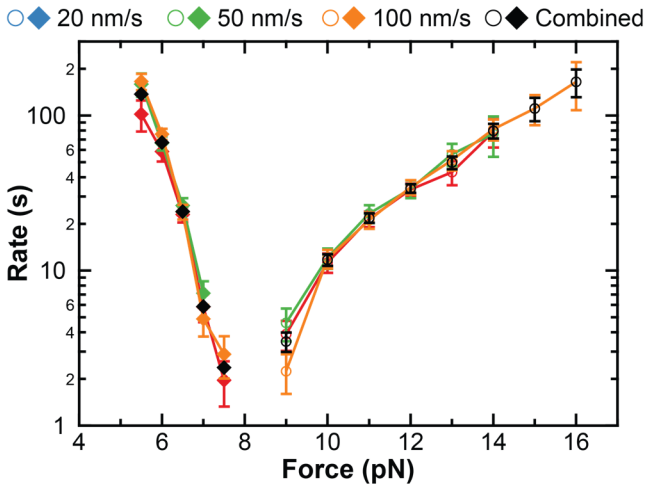

Fig. S6. Rate maps consistent across different pulling velocities. Rates for folding (filled diamonds) and unfolding (open circles) plotted as a function of force for a single molecule measured at pH 6.2. Rates were calculated from experiments pulling at v = 20 nm/s (blue, N_{cycles} = 47); v = 50 nm/s (green, N_{cycles} = 71); v = 100 nm/s (orange, N_{cycles} = 189). Average rates derived from combining the three pulling velocities shown in black. Error bars represent SEM calculated from bootstrapping.

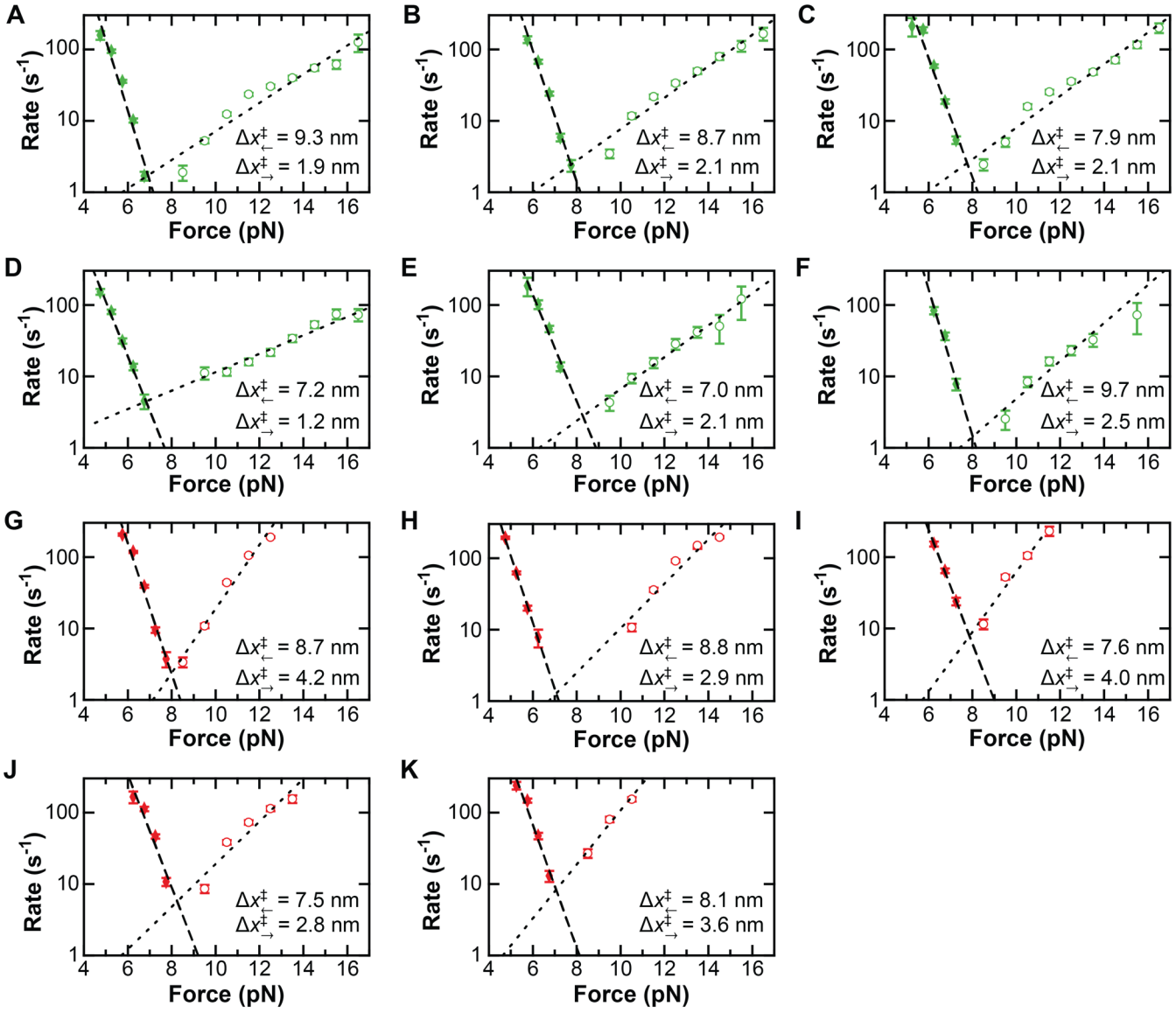

Fig. S7: Analysis of rate maps from individual molecules quantified. Rates for folding (filled diamonds) and unfolding (open circles) plotted as a function of force for single molecules measured at pH 6.2 (**A**–**F**, green), and pH 4.2 (**G**–**K**, red). Rates were calculated by combining traces folding and unfolding α_3D at v = 20, 50, and 100 nm/s. Folding and unfolding rates were then fit to the Bell model (line) and the resulting distances to the unfolding ($\Delta x^{\ddagger}_{\rightarrow}$) and folding ($\Delta x^{\ddagger}_{\leftarrow}$) transition state are indicated.

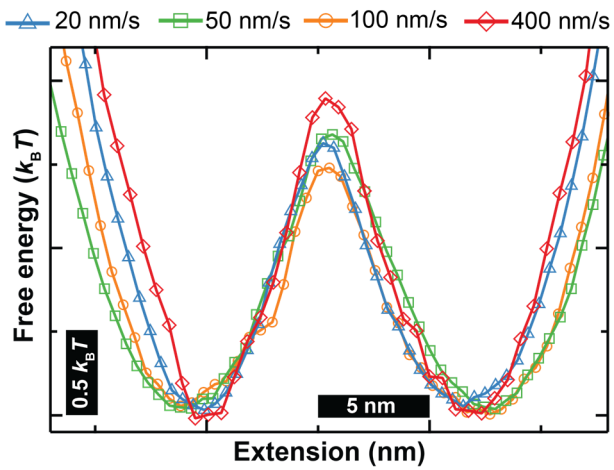

Fig. S8. Landscape reconstruction tilted to $F_{1/2}$ consistent across multiple pulling velocities. Folding free-energy landscapes for an individual molecule of α_3D molecule derived by applying the inverse Weierstrass transform to sets of stretching/relaxing cycles, each set at a constant velocity [v = 20 nm/s (N_{cycles} = 19), v = 50 nm/s (N_{cycles} = 35), v = 100 nm/s (N_{cycles} = 23), v = 400 nm/s (N_{cycles} = 50)].

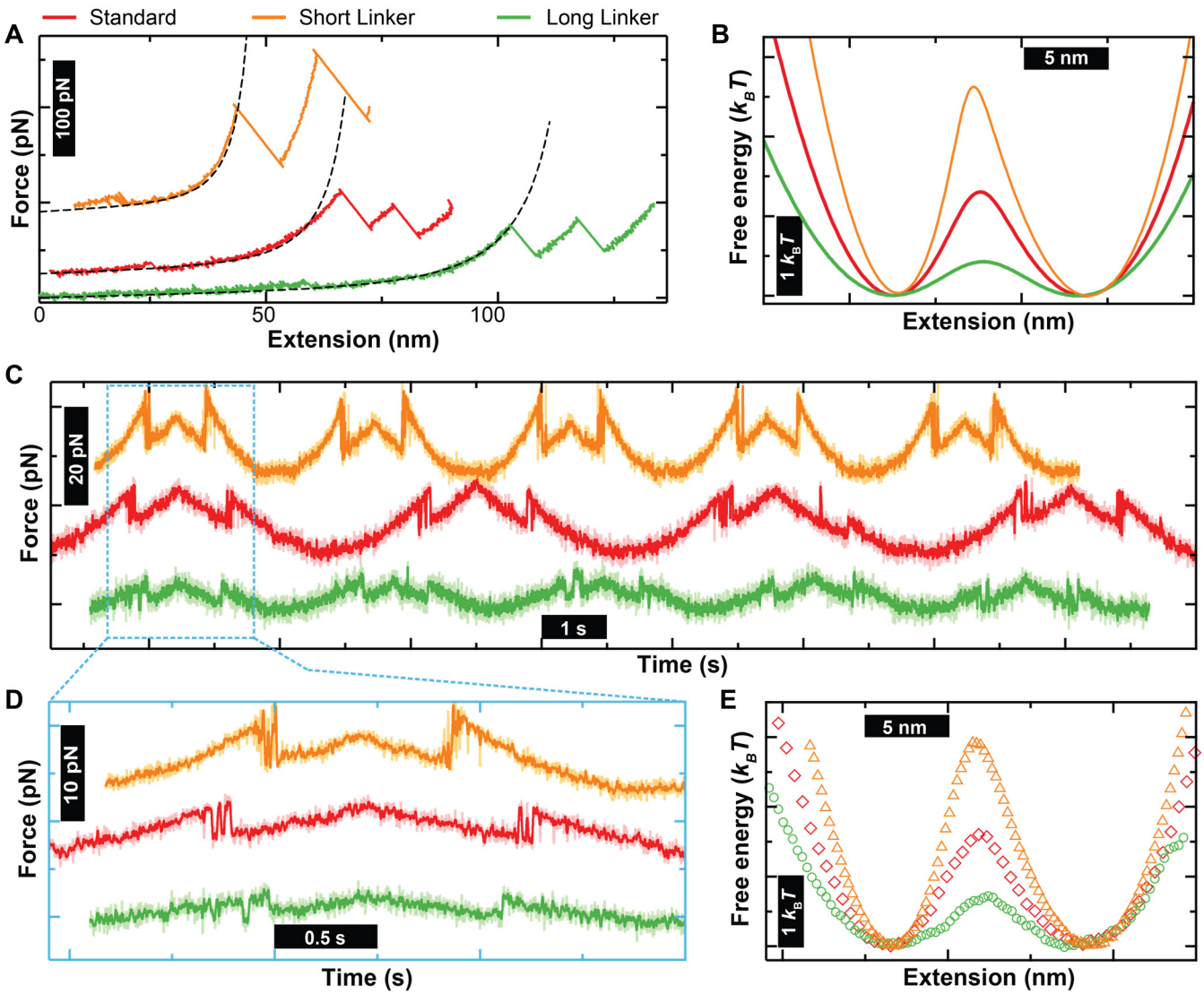

Fig. S9. Linker length affects data quality and reconstructed landscapes. (**A**) Force-extension curves for three different linker lengths with WLC fits to the segment associated with pulling on the polyprotein after α_3D unfolded but while both NuG2 domains remained folded. The middle construct (red) is a typical unfolding curve from our standard polyprotein (Fig. 2*A*). The shortest construct was an anomalously short connection to our standard polyprotein, which we attribute to manufacturing limitation of the PEG linkers. The longest construct resulted from adding an additional elastin-like polypeptide (6) to the standard polyprotein (Fig. 2*A*). (**B**) Entropic landscapes at $F_{1/2}$ calculated for the short, medium, and long linkers. The parameters used here are the same as used in the main text except with varying initial contour lengths. (**C**) Force-vs-time plots comparing folding and unfolding using short, medium, and long linkers. (**D**) High-resolution, force-vs-time plot for a single unfolding and refolding cycle. (**E**) Reconstructed free-energy landscapes determined by the inverse Weierstrass transform for the three different length constructs shown in panel C tilted to $F_{1/2}$.

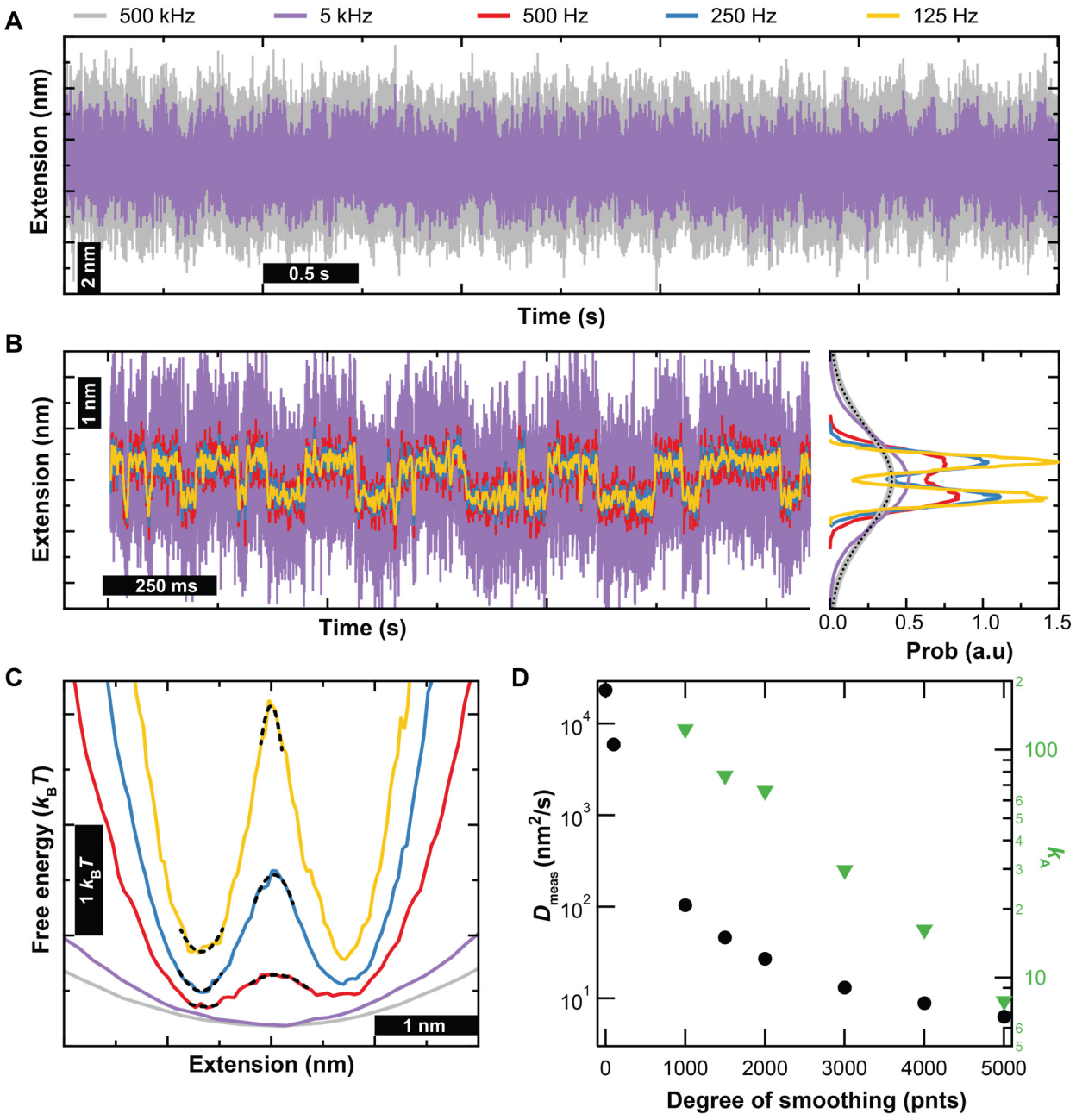

Fig. S10. Reconstructed landscapes from inverse Boltzmann vary systematically with degree of smoothing. (**A**) Extension-vs-time traces show equilibrium folding and unfolding of α_3D at 500 kHz (grey) and smoothed to 5 kHz (purple). (**B**) Extension-vs-time trace smoothed to 5000 (purple), 500 (red), 250 (blue), and 125 Hz (yellow) with histograms of $P(x)$ at each degree of smoothing shown on the right hand side. A dashed black line shows the unfiltered, 500-kHz data is well described by a Gaussian. (**C**) Free-energy landscapes calculated from an inverse Boltzmann analysis at different degrees of smoothing in the absence of deconvolution. Dashed black lines indicate a quadratic fit used to determine the stiffnesses of the wells and the barrier. (**D**) The calculated D_{meas} (left axis, black) and k_A (right axis, green) as a function of the degree of smoothing using the formulism of Cossio *et al.* (20) where 501 pnts of smoothing corresponds to 1 kHz.

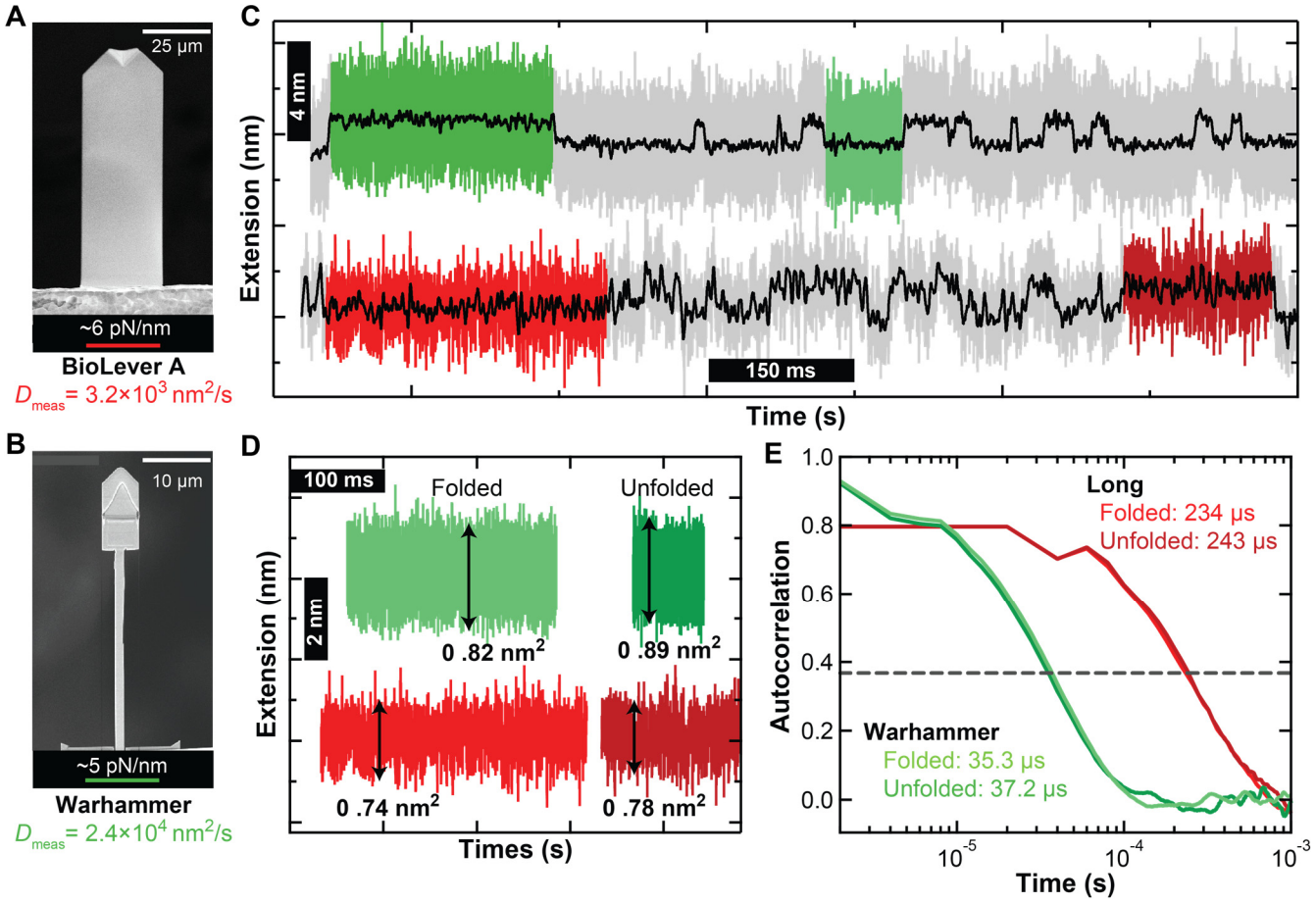

Fig. S11. Measuring diffusion coefficients of assay. (**A**) SEM image of a BioLever Long cantilever along with its spring constant and effective diffusion coefficient (D_{meas}) based on the formalism of Cossio *et al.* (20). Specifically, D_{meas} was calculated using $D_{\text{meas}} = \left\langle \partial x^2_{\text{meas}} \right\rangle / \tau$ where $\partial x^2_{\text{meas}}$ is the variance in x_{meas} in the folded and unfolded state and τ is the autocorrelation time of x_{meas} in each state. (**B**) SEM image of a Warhammer cantilever and its associated values. (**C**) Extension-vs-time traces for equilibrium folding/unfolding of α_3D acquired with a Warhammer (top trace) and a BioLever Long (bottom trace). For the Warhmmer 500 kHz data is shown, while the data from the BioLever Long is at 50 kHz. Data in black smoothed to 200 Hz. (**D**) Extracted extension-vs-time traces for the folded and unfolded states for the Warhammer (green) and BioLever Long (red) and the $\partial x^2_{\text{meas}}$ calculated from each noted. (**E**) Autocorrelation calculated from the extracted extension data where the reported autocorrelation time was determined by where the curve drops to e^{-1}.

References

1. J. Yin*, et al.*, Genetically encoded short peptide tag for versatile protein labeling by Sfp phosphopantetheinyl transferase. *Proc. Natl. Acad. Sci. U.S.A.* **102**, 15815-15820 (2005).
2. M. Schlierf, F. Berkemeier, M. Rief, Direct observation of active protein folding using lock-in force spectroscopy. *Biophysical Journal* **93**, 3989-3998 (2007).
3. C. Schoeler*, et al.*, Mapping mechanical force propagation through biomolecular complexes. *Nano Lett.* **15**, 7370-7376 (2015).
4. D. G. Gibson*, et al.*, Enzymatic assembly of DNA molecules up to several hundred kilobases. *Nat. Methods* **6**, 343-345 (2009).
5. D. T. Edwards, J. K. Faulk, M. A. LeBlanc, T. T. Perkins, Force spectroscopy with 9-μs resolution and sub-pN stability by tailoring AFM cantilever geometry. *Biophys. J.* **113**, 2595-2600 (2017).
6. W. Ott*, et al.*, Elastin-like polypeptide linkers for single-molecule force spectroscopy. *ACS Nano* **11**, 6346-6354 (2017).
7. F. W. Studier, Stable expression clones and auto-induction for protein production in E. coli. *Methods Mol. Biol.* **1091**, 17-32 (2014).
8. R. Proksch, T. E. Schaffer, J. P. Cleveland, R. C. Callahan, M. B. Viani, Finite optical spot size and position corrections in thermal spring constant calibration. *Nanotechnology* **15**, 1344-1350 (2004).
9. J. K. Faulk, D. T. Edwards, M. S. Bull, T. T. Perkins, Improved force spectroscopy using focused-ion-beam-modified cantilevers. *Methods Enzymol.* **582**, 321-351 (2017).
10. R. Walder*, et al.*, Rapid characterization of a mechanically labile α-helical protein enabled by efficient site-specific bioconjugation. *J. Am. Chem. Soc.* **139**, 9867–9875 (2017).
11. C. Schoeler*, et al.*, Ultrastable cellulosome-adhesion complex tightens under load. *Nat. Commun.* **5**, 5635 (2014).
12. R. Walder, W. J. Van Patten, A. Adhikari, T. T. Perkins, Going vertical to improve accuracy in AFM-based single-molecule force spectroscopy *ACS Nano* **12**, 198−207 (2018).
13. M. Carrion-Vazquez*, et al.*, Mechanical and chemical unfolding of a single protein: a comparison. *Proc. Natl. Acad. Sci. U.S.A.* **96**, 3694-3699 (1999).
14. M. S. Bull, R. M. Sullan, H. Li, T. T. Perkins, Improved single molecule force spectroscopy using micromachined cantilevers. *ACS Nano* **8**, 4984-4995 (2014).
15. M. Otten*, et al.*, From genes to protein mechanics on a chip. *Nat. Methods* **11**, 1127-1130 (2014).
16. D. B. Sullivan, D. W. Allan , D. A. Howe, E. L. Walls, *Characterization of Clocks and Oscillators* (U.S. Government Printing Office, Washington), (1990).
17. D. R. Jacobson, T. T. Perkins, Correcting molecular transition rates measured by single-molecule force spectroscopy for limited temporal resolution. *Phys. Rev. E* **102**, 022402 (2020).
18. Y. J. Zhang, O. K. Dudko, A transformation for the mechanical fingerprints of complex biomolecular interactions. *Proc. Natl. Acad. Sci. U.S.A.* **110**, 16432-16437 (2013).
19. H. Yu, D. R. Jacobson, H. Luo, T. T. Perkins, Quantifying the native energetics stabilizing bacteriorhodopsin by single-molecule force spectroscopy. *Phys. Rev. Lett.* **124**, 068102 (2020).
20. P. Cossio, G. Hummer, A. Szabo, On artifacts in single-molecule force spectroscopy. *Proc. Natl. Acad. Sci. U.S.A.* **112**, 14248–14253 (2015).

21. K. Neupane, M. T. Woodside, Quantifying instrumental artifacts in folding kinetics measured by single-molecule force spectroscopy. *Biophys. J.* **111**, 283-286 (2016).
22. K. Svoboda, S. M. Block, Biological applications of optical forces. *Annu. Rev. Biophys. Biomol. Struct.* **23**, 247-285 (1994).
23. H. A. Kramers, Brownian motion in a field of force and the diffusion model of chemical reactions. *Physica* **7**, 284-304 (1940).
24. R. Walder*, et al.*, High-precision single-molecule characterization of the folding of an HIV RNA hairpin by atomic force microscopy. *Nano Lett.* **18**, 6318-6325 (2018).
25. G. Hummer, A. Szabo, Free energy profiles from single-molecule pulling experiments. *Proc. Natl. Acad. Sci. U.S.A.* **107**, 21441-21446 (2010).
26. Y. Seol, J. Li, P. C. Nelson, T. T. Perkins, M. D. Betterton, Elasticity of short DNA molecules: Theory and experiment for contour lengths of 0.6-7 μm. *Biophys. J.* **93**, 4360-4373 (2007).
27. M. D. Wang, H. Yin, R. Landick, J. Gelles, S. M. Block, Stretching DNA with optical tweezers. *Biophys. J.* **72**, 1335-1346 (1997).